



THE UNIVERSITY *of* EDINBURGH

Edinburgh Research Explorer

Ca²⁺ activity signatures of myelin sheath formation and growth in vivo

Citation for published version:

Baraban, M, Koudelka, S & Lyons, DA 2017, 'Ca²⁺ activity signatures of myelin sheath formation and growth in vivo' Nature Neuroscience. DOI: 10.1038/s41593-017-0040-x

Digital Object Identifier (DOI):

[10.1038/s41593-017-0040-x](https://doi.org/10.1038/s41593-017-0040-x)

Link:

[Link to publication record in Edinburgh Research Explorer](#)

Document Version:

Peer reviewed version

Published In:

Nature Neuroscience

General rights

Copyright for the publications made accessible via the Edinburgh Research Explorer is retained by the author(s) and / or other copyright owners and it is a condition of accessing these publications that users recognise and abide by the legal requirements associated with these rights.

Take down policy

The University of Edinburgh has made every reasonable effort to ensure that Edinburgh Research Explorer content complies with UK legislation. If you believe that the public display of this file breaches copyright please contact openaccess@ed.ac.uk providing details, and we will remove access to the work immediately and investigate your claim.



1 **Ca²⁺ activity signatures of myelin sheath formation and growth *in vivo***

2

3

4

5 Marion Baraban¹, Sigrid Koudelka¹ and David A Lyons¹.

6

7

8

9

10 1. Centre for Neuroregeneration, Centre for Discovery Brain Sciences, University of Edinburgh, 49 Little

11 France Crescent, Edinburgh EH16 4SB, UK.

12

13

14

15 Correspondence prior to publication to David A Lyons (david.lyons@ed.ac.uk) and after publication to

16 either David A Lyons or Marion Baraban (marion.baraban@ed.ac.uk)

17

18

19

20 During myelination, individual oligodendrocytes initially over-produce short myelin sheaths that are
21 either retracted or stabilised. By live imaging oligodendrocyte Ca^{2+} activity *in vivo*, we find that high-
22 amplitude long-duration Ca^{2+} transients in sheaths prefigure retractions, mediated by calpain.
23 Following stabilisation, myelin sheaths grow along axons, and we find that higher frequency Ca^{2+}
24 transient activity in sheaths precedes faster elongation. Our data implicate local Ca^{2+} signalling in
25 regulating distinct stages of myelination.

26

27

28 Dynamic regulation of myelination by oligodendrocytes in the central nervous system (CNS) is essential
29 for nervous system development and life-long function¹, but our understanding of myelin sheath
30 formation and growth is limited. Zebrafish are well suited to studying the dynamics of CNS myelination
31 *in vivo*, due to their capacity for non-invasive longitudinal imaging. Previous imaging studies using
32 zebrafish have shown that individual oligodendrocytes initiate formation and elongation of their
33 myelin sheaths within a critical period of about 5 hours^{2,3}, mirroring hours-long myelin sheath
34 generation by mammalian oligodendrocytes *in vitro*⁴. During sheath formation, myelinating
35 oligodendrocytes initially overproduce short myelin sheaths (circa 5 μm in length), with some stabilised,
36 and others fully retracted^{2,3,5,6}. Following stabilisation, myelin sheaths grow along and around
37 associated axons³, to achieve dimensions that mediate the timing of impulse conduction and thus
38 neural circuit function⁷. Although axonal signals, including neuronal activity, can regulate the formation
39 and growth of myelin sheaths (e.g.^{5,8-10}), the localised signalling mechanisms that control the dynamics
40 of myelination by oligodendrocytes remain to be elucidated.

41 Ca^{2+} is a second messenger that regulates many events, and localised Ca^{2+} activity has been observed
42 in oligodendrocyte precursor cells¹¹, myelinating oligodendrocytes¹⁰, and even in mature myelin
43 sheaths¹² *in vitro* and *ex vivo*. We reasoned that determining how localised Ca^{2+} activity relates to the
44 formation and growth of myelin sheaths *in vivo* would provide novel insights into mechanisms of CNS
45 myelination.

46

47

48 To visualise Ca^{2+} activity in myelinating oligodendrocytes, we used the genetically encoded calcium
49 indicator GCaMP6s¹³, which we expressed in oligodendrocytes by crossing Tg(sox10:KaITa4) and
50 Tg(uas:GCaMP6s) transgenic zebrafish lines (Online Methods). We imaged GCaMP6s expressing
51 oligodendrocytes in the spinal cord of zebrafish larvae between 3-4 days post fertilisation (dpf), as
52 myelin sheaths are being formed and starting to elongate^{2,3}. We first assessed the kinetics of individual

53 localised Ca^{2+} transients in myelin sheaths by high-speed 2D (4Hz) imaging, and found that essentially
54 all transients lasted longer than 3.5 seconds (Supplementary Fig. 1, Supplementary Movie 1).
55 Therefore, we 3D imaged Ca^{2+} activity in all myelin sheaths belonging to individual oligodendrocytes
56 with a time interval of 2.5 seconds (Fig. 1A-E, Online Methods, Supplementary Fig. 2, and
57 Supplementary Movies 2 and 3).

58

59 To correlate Ca^{2+} activity with myelination, we time-lapse imaged individual GCaMP6s-expressing
60 oligodendrocytes for multiple 20 minute blocks over a 5-9 hour period during which they initiated
61 formation and elongation of their myelin sheaths (Fig. 1F,G). Prior to each Ca^{2+} imaging block, we
62 acquired a high-resolution 3D z-stack of GCaMP6s-expressing oligodendrocytes together with
63 *sox10:mRFP*, which allowed assessment of sheath morphology (Fig. 1F,G and see Online Methods). We
64 quantified the Ca^{2+} activity of 305 sheaths of 18 oligodendrocytes in 18 animals. Analyses of 448 Ca^{2+}
65 transients in the 187 sheaths that exhibited activity (out of the 305 sheaths imaged) revealed significant
66 diversity in the frequency (Fig.1H), amplitude and duration of transients between sheaths (Fig. 1I,J)
67 (Median amplitude per sheath $\Delta F/F_0 = 0.7$, IQR=0.9; Median Ca^{2+} transient duration= 23s, IQR=17
68 seconds per sheath). We also found that duration and amplitude were positively correlated, whereby
69 longer duration transients tended to also be of higher amplitude (Fig. 1K).

70

71 The diversity in Ca^{2+} transient activity between sheaths suggested that their frequency, duration and/or
72 amplitude may influence myelination. We first focussed on the relationship between Ca^{2+} activity and
73 myelin sheath formation. We found that 61 of the 305 sheaths analysed were completely retracted
74 during our imaging protocol, reflecting the initial over-production of sheaths. Intriguingly, we found
75 that the amplitude of Ca^{2+} transients in sheaths that were subsequently retracted was three-fold higher
76 than in those sheaths that were stabilised (Fig. 2A,B,D: Median amplitude =1.8 $\Delta F/F_0$ in fully retracted
77 sheaths vs 0.6 $\Delta F/F_0$ in stabilised sheaths). Furthermore, we observed an increase in Ca^{2+} transient
78 duration in sheaths that were subsequently retracted (Fig.2C,D: Median duration= 35s in retracted
79 sheaths vs 22s in stabilised). Interestingly, the Ca^{2+} transients observed in sheaths that were
80 subsequently retracted travelled from sheath to process (Supplementary Fig. 3, Supplementary Movie
81 4), reflecting the directionality of retraction, first of the sheath and then the process (Fig. 2A,
82 Supplementary Fig. 4). These observations lead us to hypothesise that localised high-amplitude long-
83 duration Ca^{2+} transients may mediate sheath retraction through activation of Ca^{2+} -dependent
84 mechanisms.

85

86 We hypothesised that calpain enzymes, Ca^{2+} dependent non-lysosomal proteases, might mediate
87 sheath retraction. Calpains underpin many aspects of cellular breakdown, including the localised
88 pruning of dendrites in *Drosophila* following large Ca^{2+} transients¹⁴. To test whether calpain mediates
89 myelin sheath retractions, we took chemical and genetic approaches. We first treated animals with the
90 calpain inhibitor PD150606¹⁵ from 2-4 dpf, and assessed the morphology of individual
91 oligodendrocytes with *mbp:mCherry-CAAX*⁶. We found that PD150606 treatment increased myelin
92 sheath number per oligodendrocyte (Fig. 2E,H) (Average sheath number per oligodendrocyte: DMSO
93 14.4 ± 3.2 vs PD150606 18.7 ± 5.9). In order to whether calpain actually mediates retraction of sheaths,
94 we carried out time-lapse microscopy of PD150606-treated animals. These studies revealed a lower
95 rate of sheath retraction in calpain-inhibited animals during the dynamic period of sheath stabilisation
96 and retraction (Fig. 2F,I and Supplementary movies 5+6) (Sheath retraction per oligodendrocyte per
97 hour, DMSO 0.34 ± 0.13 vs PD150606 0.24 ± 0.13). To independently and cell autonomously test the role
98 for calpain in regulating myelin sheath number, we expressed the endogenous inhibitor of calpain,
99 calpastatin¹⁶, in myelinating oligodendrocytes (see Online Methods and Supplementary Fig. 5). Analysis
100 of oligodendrocyte morphology revealed that cell-type specific disruption of calpain protease function
101 increased the number of myelin sheaths compared to control (Fig. 2G,J) (Average sheath number per
102 cell *mbp:meGFP* 15.8 ± 6.4 vs *mbp:meGFP-calpastatin* 20.5 ± 5.8).

103 Together, these data support our imaging-driven hypothesis that calpain regulates retraction of myelin
104 sheaths during the dynamic period of myelin sheath formation by individual oligodendrocytes.

105

106 We next assessed how Ca^{2+} transient activity might relate to myelin sheath growth. By comparing Ca^{2+}
107 activity and differential growth over time (Fig. 3A,B), we found that the frequency of the lower
108 amplitude shorter duration Ca^{2+} transients observed in stabilised sheaths correlated positively with the
109 speed of sheath elongation (Fig. 3C,D). Interestingly, when we analysed how individual sheaths grew
110 after each Ca^{2+} transient, we observed positive elongation within the first 2 hours of the Ca^{2+} transient
111 (Fig. 3E). We did not see any correlation between the average amplitude or duration of transients with
112 the speed of growth (Supplementary Fig. 6). These observations show the frequency of low amplitude
113 short duration Ca^{2+} transients in stabilised sheaths is predictive of their speed of elongation, suggesting
114 that dynamic changes in myelin sheath Ca^{2+} concentration regulate sheath growth.

115

116 Our live imaging has revealed distinct signatures of localised Ca^{2+} activity during CNS myelination. High-
117 amplitude long duration Ca^{2+} transients precede localised retraction of sheaths, mediated by calpain,
118 whereas the frequency of lower amplitude shorter duration transients in stabilised sheaths correlates

119 positively with their speed of elongation (Summarised in Supplementary Fig. 7). How could distinct Ca^{2+}
120 signatures lead to such different outcomes during myelination? With respect to sheath retraction, it is
121 known that different isoforms of calpain have distinct sensitivities to Ca^{2+} concentration, with some
122 primed for activation by localised changes in Ca^{2+} concentration¹⁷. It is possible that large localised
123 increases in Ca^{2+} concentration following individual high-amplitude long-duration transients could
124 stimulate local protease activity that leads to sheath retraction, e.g. by localised degradation of
125 cytoskeletal components. With respect to the speed of sheath elongation, it is now known that myelin
126 sheath growth occurs is driven at inside of the myelin sheath³, at least in part, by iterative cycles of
127 actin polymerisation and depolymerisation¹⁸. Given that actin polymerisation/depolymerisation can be
128 regulated by Ca^{2+} , it is possible that localised changes in Ca^{2+} concentration could affect the speed of
129 sheath growth via regulating the actin cytoskeleton.

130

131 Many additional questions remain as to how localised Ca^{2+} regulates myelination. Which signal(s) lead
132 to the distinct changes in myelin sheath Ca^{2+} during retraction, stabilisation and growth? Neuronal
133 activity is one signal known to affect myelination^{5,8-10}, and many of its candidate mediators in
134 oligodendrocytes converge on regulation of intracellular Ca^{2+} ¹⁹. Indeed, a complementary study to
135 ours indicates that neuronal activity regulates about half of the Ca^{2+} transients in myelin²⁰. How Ca^{2+}
136 might affect ongoing sheath growth and remodelling throughout life, and during regeneration, also
137 remain to be investigated. We anticipate that live Ca^{2+} imaging-focused approaches will continue to
138 elucidate the mechanisms underlying the dynamic regulation of myelination in the CNS.

139

140 **Accession codes**

141 The Genbank accession number for *calpastatin* mRNA is MG387170.

142

143 **Author contributions**

144 MB designed and performed experiments and co-wrote manuscript. SK performed experiments using
145 chemical inhibitors. DAL designed experiments, managed project and co-wrote manuscript.

146

147 **Acknowledgements**

148 We would like to thank members of the Lyons lab, as well as Thomas Becker, Peter Brophy, Charles
149 ffrench-Constant, Matthew Livesey, Dies Meijer, Will Talbot and Claire Wyart for helpful comments on
150 the manuscript. We would like to thank Herwig Baier for transgenic zebrafish, Bertrand Vernay for

151 support in image analysis. This work was supported by a Lister Institute Research Prize and a Wellcome
152 Trust Senior Research Fellowship (102836/Z/13/Z) to DAL.

153

154 **Competing financial interests**

155 I declare that the authors have no competing interests as defined by Springer Nature, or other interests
156 that might be perceived to influence the results and/or discussion reported in this paper.

157

158

159 **References**

- 160 1. Chang, K.-J., Redmond, S.A. & Chan, J.R. *Nat Neurosci* **19**, 190–197 (2016).
- 161 2. Czopka, T., Ffrench-Constant, C. & Lyons, D.A. *Developmental Cell* **25**, 599–609 (2013).
- 162 3. Snidero, N. et al. *Cell* **156**, 277–290 (2014).
- 163 4. Watkins, T.A., Emery, B., Mulinyawe, S. & Barres, B.A. *Neuron* **60**, 555–569 (2008).
- 164 5. Hines, J.H., Ravanelli, A.M., Schwandt, R., Scott, E.K. & Appel, B. *Nat Neurosci* **18**, 683–689
165 (2015).
- 166 6. Mensch, S. et al. *Nat Neurosci* **18**, 628–630 (2015).
- 167 7. Fields, R.D. *Nat Rev Neurosci* **16**, 756–767 (2015).
- 168 8. Wake, H. et al. *Nature Communications* **6**, 7844 (2015).
- 169 9. Koudelka, S. et al. *Curr. Biol.* **26**, 1447–1455 (2016).
- 170 10. Wake, H., Lee, P.R. & Fields, R.D. *Science* **333**, 1647–1651 (2011).
- 171 11. Sun, W., Matthews, E.A., Nicolas, V., Schoch, S. & Dietrich, D. *Elife* **5**, (2016).
- 172 12. Micu, I. et al. *Experimental Neurology* **276**, 41–50 (2016).
- 173 13. Chen, T.-W. et al. *Nature* **499**, 295–300 (2013).
- 174 14. Kanamori, T. et al. *Science* **340**, 1475–1478 (2013).
- 175 15. Wang, K.K. et al. *PNAS* **93**, 6687–6692 (1996).
- 176 16. Moldoveanu, T., Gehring, K. & Green, D.R. *Nature* **456**, 404–408 (2008).
- 177 17. Campbell, R.L. & Davies, P.L. *Biochem. J.* **447**, 335–351 (2012).
- 178 18. Nawaz, S. et al. *Developmental Cell* **34**, 139–151 (2015).
- 179 19. Pitman, K.A. & Young, K.M. *Int. J. Biochem. Cell Biol.* **77**, 30–34 (2016).

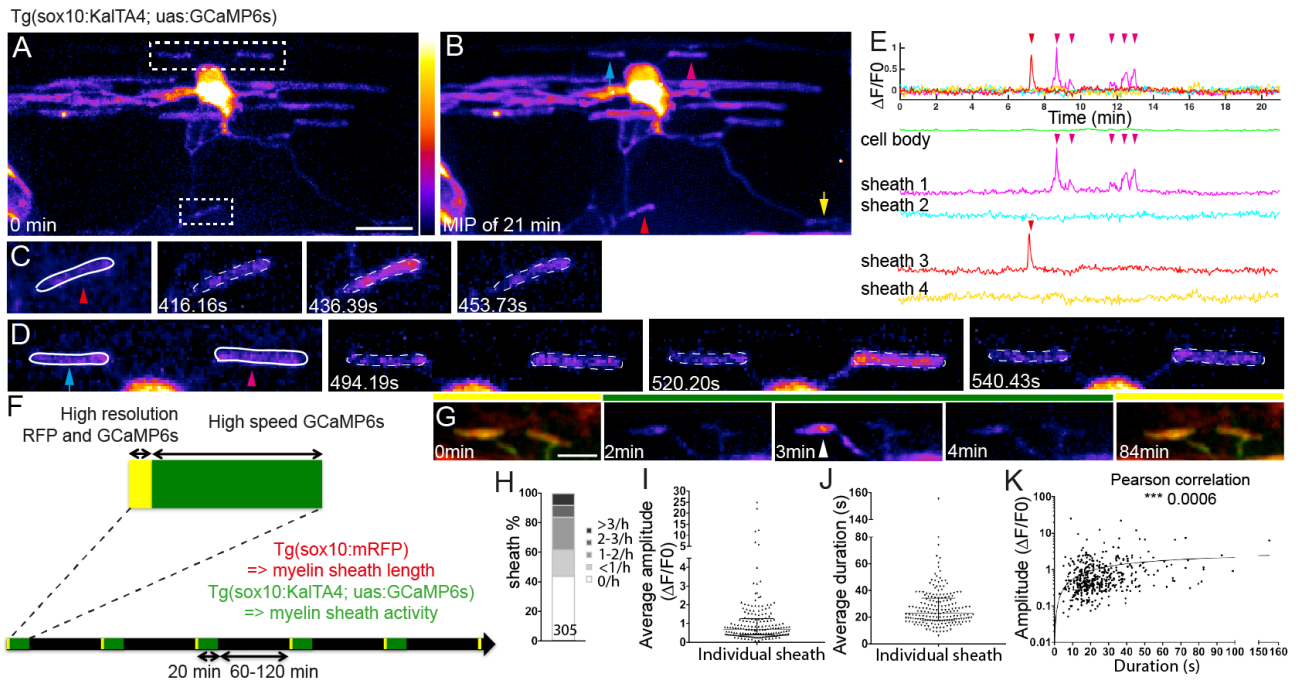
180 20

181

182

183

184



185

186 **Figure 1. Live imaging reveals localised Ca^{2+} activity in newly forming myelin sheaths**

187 A. Maximum intensity projection of a 3D z-stack of the first time-point from a 21 minute-long movie of
 188 a GCaMP6s expressing oligodendrocyte. Two areas of interest indicated, top corresponding to D and
 189 bottom to C. Scale bar= 10 μm . Fire LookUpTable.

190 B. Maximum intensity projection of all time-points of cell shown in A. Arrowheads indicate sheaths
 191 with increased fluorescence, reflecting Ca^{2+} activity during the movie. Arrows point to sheaths with no
 192 increase.

193 C, D, myelin sheaths demarcated within ROIs outlined in A, at indicated times.

194 E. $\Delta\text{F}/\text{F}_0$ over time. Arrowheads indicate sheaths shown in corresponding colours in B, C and D.

195 F. Schematic of time-lapse imaging experiment with interspersed imaging of cell morphology (yellow)
 196 and Ca^{2+} (green).

197 G. Sample images of myelin sheath morphology (under yellow bars) with intervening periods of Ca^{2+}
 198 imaging (under green bar). Arrowhead points to Ca^{2+} transient in sheath. Scale bar=5 μm .

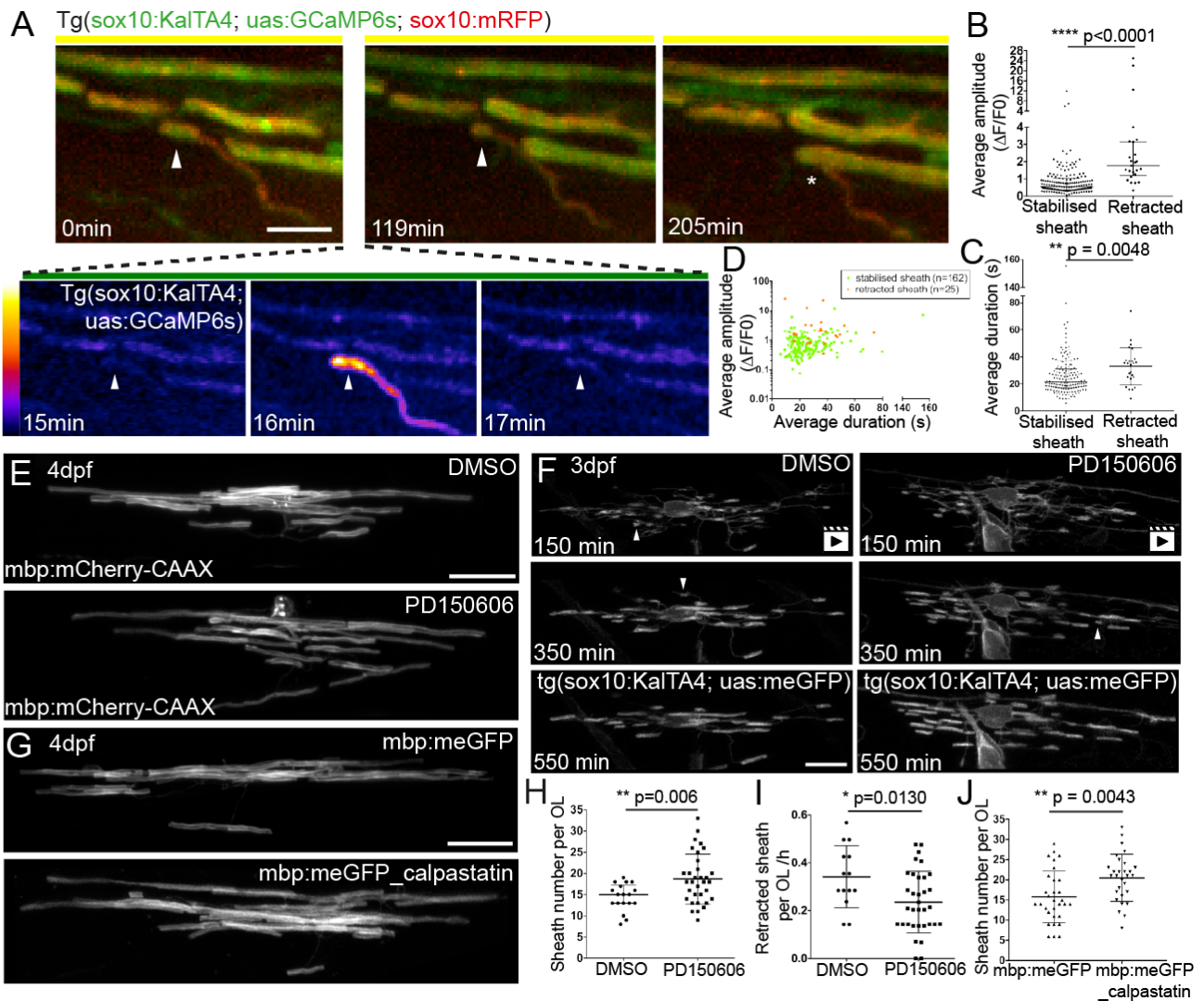
199 H. Distribution of Ca^{2+} transient frequencies of 305 sheaths, analysed in 18 animals.

200 I. Distribution of average Ca^{2+} transient amplitude per sheath (187 sheaths from 18 animals). Graph
 201 shows median and 1st and 3rd quartiles.

202 J. Distribution of average Ca^{2+} transient duration per sheath (187 sheaths from 18 animals). Graph
 203 shows median and 1st and 3rd quartiles.

204 K. Correlation between amplitude and duration per individual Ca^{2+} transient events (448 events from
 205 187 sheaths in 18 animals, Pearson's Correlation Test, $p=0.0006$).

206



207

208 **Figure 2. High-amplitude long duration Ca^{2+} transients precede calpain-driven sheath retractions.**

209 A. Frames from a time-lapse imaging experiment. The myelin sheath imaged in high-resolution mode
 210 (0 min) exhibits a Ca^{2+} transient 16 minutes into a period of high-speed GCaMP6s imaging (see also
 211 Supplementary Fig. 3) subsequently retracts, first along the length of the axon (119 min) and then
 212 entirely from the axon (205 min, asterisk). Scale bar= 5 μ m.

213 B. Average amplitude of Ca^{2+} transients in sheaths that are either stabilised or fully retracted (n=25
 214 retracted sheaths, 12 animals and n=162 stabilised sheaths, 18 animals; Graph shows median and 1st
 215 and 3rd quartiles. Two-tailed Mann-Whitney test, p<0.0001.

216 C. Average duration of Ca^{2+} transients in sheaths shown in B. Graph shows median and 1st and 3rd
 217 quartiles. Two-tailed Mann-Whitney test, p=0.0048.

218 D. Average amplitude and average duration of transient events in sheaths that are stabilised (green)
 219 or fully retracted (orange).

220 E. mbp:mCherry-CAAX expressing oligodendrocytes in control (top) and PD150606 treated animal
 221 (bottom) at 4 dpf. Scale bar= 10 μ m. Quantitation in 2H.

222 F. Frames from time-lapse movies of oligodendrocytes during myelination in a DMSO treated (left) and
223 PD150606 treated (right) animal. Arrowheads point to sheaths that are retracted. See also
224 Supplementary Movies 5+6. Scale bar= 10 μ m. Quantitation in 2I.

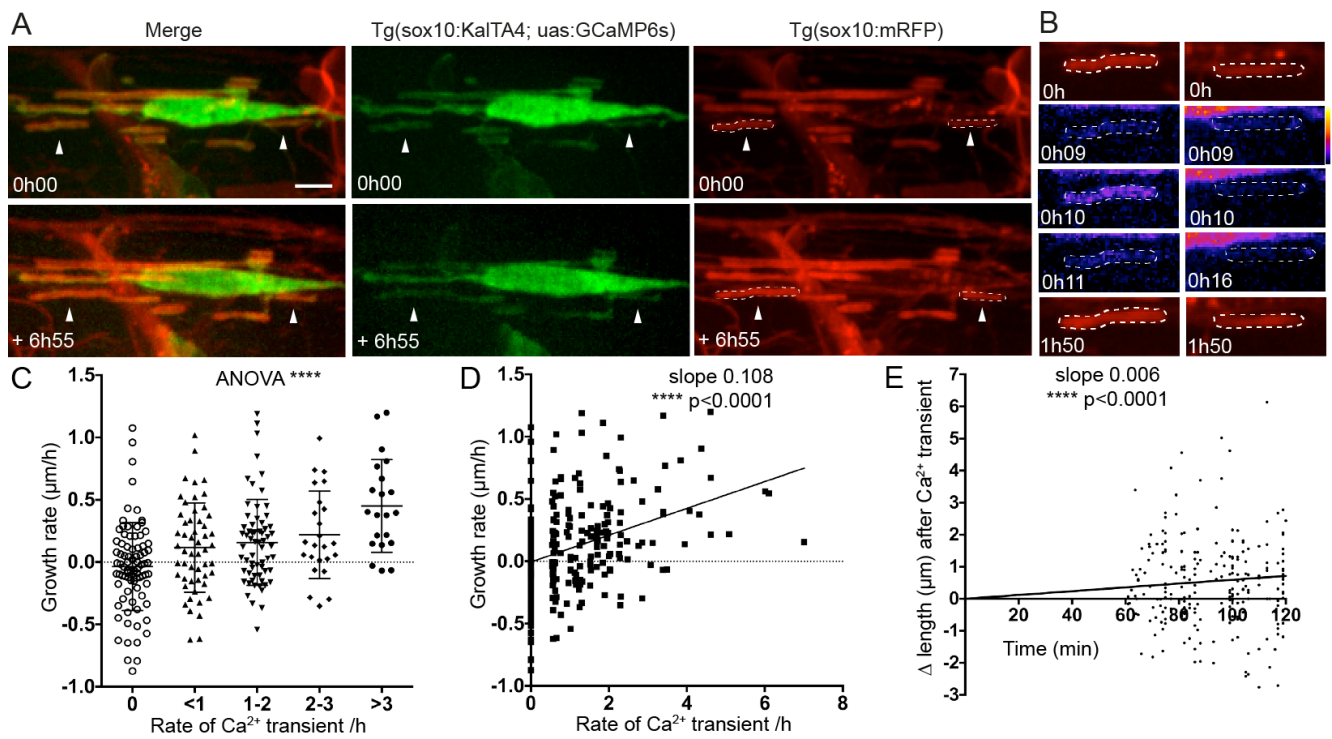
225 G. mbp:meGFP expressing oligodendrocytes (top) and mbp:meGFP-calpastatin (bottom) at 4 dpf. Scale
226 bar= 10 μ m. Quantitation in 2J.

227 H. Myelin sheath number per oligodendrocyte in DMSO and PD150606 treated animals (n=18 OLs from
228 18 DMSO-treated animals; n= 33 OLs from 33 PD150606-treated animals; Graph shows mean and SD.
229 Two-tailed t-test, p=0.006).

230 I. Rate of myelin sheath retraction per hour in DMSO and PD150606 treated animals as analysed by
231 time-lapse microscopy. (n=14 OLs from 14 DMSO-treated animals and 34 OLs from 34 PD150606-
232 treated animals. Graph shows mean and SD. Two-tailed t-test, p=0.013).

233 J. Myelin sheath number per mbp:meGFP and mbp:meGFP-calpastatin expressing oligodendrocytes at
234 4 dpf. (n=31 OLs in 22 mbp:meGFP control animals, and n=29 OLs in 23 mbp:meGFP-calpastatin
235 animals. Graph shows mean and SD. Two-tailed t-test, p=0.0043).

236



237

238

239 **Figure 3. Ca²⁺ transient frequency correlates with sheath elongation**

240 A. Images of a GCaMP6s expressing oligodendrocyte in a Tg(sox10:mRFP) background allows analysis
 241 of the growth and Ca²⁺ activity of individual isolated myelin sheaths, e.g. arrowheads over time. Top
 242 panels show initial time-point and bottom the same cell at the end of the movie almost 7 hours later.
 243 Scale bar= 5µm.

244 B. Myelin sheaths indicated by arrowheads in A are outlined by ROIs and imaged over time. Note the
 245 Ca²⁺ transient at 0h 10 time-point in the sheath in the left column subsequently elongates.

246 C. Growth rate of myelin sheaths (µm/h) related to number of Ca²⁺ transients per hour. (ANOVA
 247 p<0.0001, F=9.225. Two-tailed unpaired t-test, 0 vs >3 transients/h p<0.0001, 0 vs 2-3 transients/h
 248 p=0.0024, 0 vs 1-2 transients/h p=0.0011, 0 vs <1 transient/h p=0.0162, <1 vs >3 transients/h p=0.0006,
 249 1-2 vs >3 transients/h p=0.0014, 2-3 vs >3 transients/h p=0.0376; 0 transient/h n=82 sheaths from 17
 250 animals, <1 transient/h n=53 from 16 animals, 1-2 transients/h n=64 sheaths from 17 animals, 2-3
 251 transients/h n=24 sheaths from 11 animals, >3 transients/h n=21 sheaths from 11 animals). Graph
 252 indicates means and standard deviations.

253 D. Scatterplot analysis of growth rate of myelin sheaths (µm/h) related to number of Ca²⁺ transients
 254 per hour (Slope= 0.108. Pearson's Correlation Test, p<0.0001, n=244 sheaths).

255 E. Change in sheath length over time following 324 Ca²⁺ transients, with the time of all transients set
 256 as time 0 (slope 0.006, Linear Regression test, p<0.0001).

257

258

259 **Online Methods**

260 **Zebrafish husbandry**

261 All animal studies were carried out with approval from the UK Home Office and according to its
262 regulations, under project licenses 60/ 8436 and 70/8436. The project was approved by the University
263 of Edinburgh Institutional Animal Care and Use Committee. We used zebrafish (*Danio rerio*) only, and
264 the following transgenic lines in this study: $\text{tg}(\text{sox10}(7.2):\text{KalTA4GI})^{21}$, $\text{tg}(\text{UAS:mem-GFP})$,
265 $\text{tg}(\text{uas:GCaMP6s})^{13}$ and $\text{tg}(\text{sox10:mRFP})^{22}$. All Ca^{2+} imaging was carried out in the nacre background²³,
266 which lack melanocytes.

267 **Image acquisition**

268 We combined stable transgenic zebrafish $\text{Tg}(\text{sox10:KalTA4})$, which drives gene expression in the
269 oligodendrocyte lineage, with $\text{Tg}(\text{uas:GCaMP6s})$ that expresses the genetically encoded calcium
270 indicator GCaMP6s under the control of 14X repetitive Upstream Activator Sequences (uas), the nacre
271 homozygous mutant line that lacks melanocytes, and also $\text{Tg}(\text{sox10:mRFP})$ which drives membrane
272 localised RFP expression in the myelinating oligodendrocyte lineage. The combination of
273 $\text{Tg}(\text{sox10:KalTA4})$ and $\text{Tg}(\text{uas:GCaMP6s})$ leads to mosaic expression of GCaMP6s in isolated cells of the
274 oligodendrocyte lineage in the CNS.

275 Prior to imaging, larvae were screened for the expression of GCaMP6s in isolated oligodendrocytes in
276 the dorsal spinal cord at 3-4 days post fertilisation (dpf). Selected larvae were paralysed using the
277 Neuromuscular Junction (NMJ) blocking nicotinic receptor antagonist pancuronium bromide (Sigma,
278 P1918), which was dissolved in embryo medium (0.15-0.3mg/ml). Larvae were then embedded in 1.3%
279 agarose for imaging. Imaging was carry out on an Olympus Revolution XDi spinning disk confocal
280 microscope using a 1.2 NA 60X water immersion objective, plus a camera zoom of 2X, giving an X-Y
281 image area of $117 \times 117 \mu\text{m}$ and acquisition at 512×512 pixels. Larvae were maintained at 28°C in
282 temperature controlled chamber (Okolab). Images were acquired using the iQ3 software (Andor) and
283 iXon EMCCD Ultra 897 camera.

284 For initial 2D characterisation of calcium transient kinetics, $\text{Tg}(\text{sox10:KalTA4}, \text{uas:GCaMP6s})$,
285 $\text{Tg}(\text{sox10:mRFP})$ larva were time-lapse imaged for periods of 10-30 min with 100ms exposure time, and
286 150-250ms intervals, reflecting imaging in one (GCaMP6s) or two (GCaMP6s and mRFP) channels, for
287 a final rate of 4-6.66 Hz (final rates also incorporate camera integration times).

288 To investigate how Ca^{2+} activity related to cell fate, $\text{Tg}(\text{sox10:KalTA4}, \text{uas:GCaMP6s}, \text{sox10:mRFP})$,
289 $\text{nacre}^{-/-}$ larva were imaged every 60-120 min as follows. First, one high-resolution 3D $29 \mu\text{m}$ deep
290 (average $\pm 2 \mu\text{m}$) z-stack of both RFP and GCaMP6s expression was acquired at 100ms exposure, 4x

291 averaging, and z-intervals between optical slices of 0.33 μ m. Immediately thereafter, 3D time-lapse
292 images of GCaMP6s expression alone were acquired of the same 29 μ m (\pm 2 μ m) volume, at 100ms
293 exposure (no averaging), and z step of 1.3 μ m. The time interval between consecutive z-stacks in the
294 time-lapse was 2.538s (\pm 0.264s), including z-positioning and camera integration times. Absolute values
295 of imaging parameters were incorporated into analyses of all individual Ca²⁺ transients and time-lapse
296 data.

297

298 **Image analysis**

299 2D time-lapse imaging data were analysed using Fiji. To correct for sample drift throughout the movie
300 we used the “Image stabilizer registration” Fiji plugin (Kang Li). Because of the very sparse labelling of
301 individual GCaMP6s expressing oligodendrocytes it is possible to identify Ca²⁺ transients by manual
302 inspection of time-lapse series. Regions of interest are then applied around all myelin sheaths and also
303 in a separate area with no GCaMP6s expression, which represents background. Then fluorescent
304 intensity measurements are extracted from both ROIs and imported into Excel. To measure $\Delta F/F_0$ we
305 apply the following formula: $\Delta F/F_0 = (F(t) - F(0)) / (F(0) - F(\text{background}))$ where F(t) is the fluorescence
306 intensity in the ROI in which the Ca²⁺ transient was observed at time (t), F(0) the average fluorescence
307 intensity of the first 4 frames of the movie in the same ROI and F(background) the fluorescence
308 intensity of the background ROI at time (t). See Supplementary Figure 1 for overview. This $\Delta F/F_0$
309 information and corresponding image acquisition parameters are imported into pClamp (Molecular
310 Devices) for detailed analyses of the duration and amplitude of individual Ca²⁺ transients.

311 For 3D time-lapse imaging data, maximum intensity projections of the individual time-points from 3D
312 time-lapse data were made using Fiji and the image stabilizer Fiji plugin was again run to account for
313 drift. In parallel 3D datasets were registered using the “Descriptor-based series registration (2d/3d+t)”
314 Fiji plugin, after which maximum intensity projections are made and Ca²⁺ transients identified
315 manually. Ca²⁺ transients were then identified manually. Only Ca²⁺ transients identified following both
316 modes of image processing were considered as valid. All myelin sheaths without overlapping structures
317 in the X-Y or Z planes were analysed. Regions of interest are then applied around all myelin sheaths
318 and corresponding background, as above. In addition, the ROI with the candidate Ca²⁺ transient was
319 moved to an immediately adjacent region in order to rule out the possibility that any, very infrequent,
320 general increase in background fluorescence in the region could identify a spurious transient. Key
321 parameters for analysis of 3D time-lapse datasets were extracted from the iQ3 metadata files using a
322 custom-written Fiji macro written by Dr. Bertrand Vernay, University of Edinburgh. These parameters

323 were then imported into Microsoft Excel for analysis. All Ca²⁺ transients were identified by $\Delta F/F(0)$ as
324 above and analysed using pClamp.

325

326 To measure myelin sheath length, we used the 3D high-resolution single time z-stack datasets acquired
327 before each period of GCaMP6s time-lapse imaging. The expression of GCaMP6s allowed identification
328 of individual myelin sheaths and the membrane localised mRFP in the same sheaths allowed more
329 accurate measurement of length.

330

331 **Calpain inhibitor treatment and analysis**

332 The calpain inhibitor PD150606 (Tocris) was applied in solution from 50 μ M -75 μ M with 1% DMSO to
333 embryos from 2-4 dpf and vehicle alone applied to controls. The morphology of myelinating
334 oligodendrocytes was assessed as previously by imaging individual oligodendrocytes expressing the
335 mbp:mCherry-CAAX reporter⁶. Images of individual myelinating oligodendrocytes were taken on a
336 Zeiss 880 with Airyscan, in animals immobilized using 1.3% Low melting point agarose with 0.03%
337 Tricaine in embryo medium. Individual myelin sheaths were identified in 3D z-stacks and measured
338 using Fiji. Time-lapse analyses were carried out using tg(sox10(7.2):KalTA4GI), tg(UAS:mem-GFP),
339 animals, which were imaged on a Zeiss 880 Airyscan in Fast Mode and with a piezo z-drive to allow
340 rapid acquisition of confocal z-stacks. Z-stack images were collected every 5 minutes for a 15 hour
341 period from 81-96 hpf.

342

343 **Cell-type specific expression of calpastatin in myelinating oligodendrocytes**

344 In order to disrupt calpain function in a cell type specific manner, we chose to express the endogenous
345 inhibitor of calpain, calpastatin²⁴, in myelinating oligodendrocytes. We first cloned zebrafish
346 calpastatin. To do so, we extracted mRNA from whole zebrafish embryos at 3 and 4 dpf, generated
347 cDNA and amplified calpastatin using the following primers castF: 5'- ATGGCGTACGCAATGTATTGG -3';
348 castR: 5'-TTATCTTTTCCAGCCTTTGTGG-3' and high fidelity Phusion polymerase (Thermo Fisher). We
349 cloned cast fragments into pCRTM-Blunt II-TOPOTM (Thermo Fisher) and Sanger sequenced clones
350 (Source Bioscience). We subcloned multiple cast mRNA variants into pCS2+ and generated synthetic
351 mRNA, which we injected into animals at the one cell stage to identify full-length version that lead to
352 an increase in myelin sheath number per oligodendrocyte in the dorsal spinal cord (Supplementary Fig.
353 5 and data not shown). We next generated a p3E vector in which full length cast was flanked by p2A
354 and a SV40 polyA sequences. We then generated a pME vector with the Fyn myristoylation domain
355 added to GFP, by amplifying GFP from pCS2+eGFP and adding the myristoylation sequence using the

356 following primer meGFPF 5'-ATGGGCTGTGTGCAATGTAAGGATAAAGAAGCAACAAAACACTGACG-3.' To
357 generate a construct for cell type specific expression of meGFP-pA or meGFP-2A-cast-pA we
358 recombined the previously described p5E-mbp plasmid containing zebrafish myelin basic protein
359 regulatory sequence²⁵, with the pME-meGFP and p3E-pA or with the pME-meGFP and p3E-2A-cast-pA.
360 mbp:meGFP-pA (5pg) or mbp:meGFP-2A-cast-p2A (10pg) plasmids were injected into zebrafish at the
361 1-2 cell stage together with 25pg tol2 mRNA²⁶. Individual oligodendrocytes were imaged at 4dpf using
362 meGFP on a Zeiss 880 Airyscan confocal microscope in Fast Mode.

363

364 **Statistics and reproducibility**

365 All data are shown as mean \pm standard deviation or median with 1st and 3rd quartiles as indicated.

366 All the statistical tests were carry out using GraphPad (Prism 6 or 7). Power calculations were calculated
367 using Statmate 2 to determine for Ca2+ imaging analyses, and investigations of the role of calpain
368 signalling in myelination. All analyses had a power >80%. Randomisation of imaging and analyses was
369 not carried out on animals whose myelin sheaths were Ca2+ imaged, as all are wildtype. For chemical
370 and genetic manipulations of calpain function, zebrafish embryos for both experimental and control
371 conditions derived from the same clutch (per experiment). For time-lapse analyses of chemical
372 inhibitor treated animals, control and experimental animals were imaged separately for technical
373 reasons. Embryos were grown up in the same incubator and the same conditions prior to analyses, all
374 live imaging. During live imaging analyses, experimental and control animals were imaged in an
375 alternating pattern (per experiment) to ensure no confounding effects of stage of development
376 between groups. The analysis of all experimental findings were carried out blinded and image data was
377 randomised using a custom-made script.

378 The data shown in Supplementary Figure 1 is representative of 20 myelin sheaths imaged in 12 animals
379 over 4 separate experimental sessions.

380 The data shown in Figure 1A-E and Supplementary Figure 2 are representative of 40 oligodendrocytes
381 imaged in 40 animals over 25 separate occasions.

382 The images analysed and data presented in Figures 1G-K, 2A-D and Figure 3 are representative of 18
383 cells imaged over 9 separate experimental sessions.

384 The images analysed and data presented in Figure 2E,H are representative of 4 experimental sessions.

385 The images analysed and data presented in Figure 2G,J are representative of 4 experimental sessions.

386 The images analysed and data presented in Figure 2F,I are representative of 6 experimental sessions.

387 Data were tested for normality by the D'Agostino & Pearson omnibus normality test. Normal
388 distributed data were tested as appropriate by two-tailed student's t-test unpaired (equal variance was
389 tested using the F test) or two-tailed one-way ANOVA (equal variance was tested using the Brown-
390 Forsythe test). Non-normally distributed data were tested by a two-tailed Mann-Whitney tests. The
391 Pearson's correlation test was used to test the correlation in Fig.1J and Fig. 3D. Linear regression
392 analyses were used to test whether the slopes differed significantly from zero in Fig. 3E. Throughout
393 all analyses * p<0.05, **p<0.01, ***p<0.001, ****p<0.0001.

394 Please see Life Sciences Reporting Summary for further details on experimental design.

395 Data and code availability

396 Transgenic constructs and transgenic zebrafish lines will be available upon request. The data that
397 support the findings of this study are available from the corresponding author upon reasonable
398 request. Custom written code for analyses of Ca²⁺ imaging data are specific to the imaging platform,
399 but details are available upon request. Custom written codes for blinding of image analyses are
400 available upon request.

401

402 **Supplementary References (Online Methods)**

- 403 21. Almeida, R.G. & Lyons, D.A. *Zebrafish* **12**, 377–386 (2015).
- 404 22. Kirby, B.B. et al. *Nat Neurosci* **9**, 1506–1511 (2006).
- 405 23. White, R.M. et al. *Cell Stem Cell* **2**, 183–189 (2008).
- 406 24. Kiss, R., Kovács, D., Tompa, P. & Perczel, A. *Biochemistry* **47**, 6936–6945 (2008).
- 407 25. Almeida, R.G., Czopka, T., Ffrench-Constant, C. & Lyons, D.A. *Development* **138**, 4443–4450
408 (2011).
- 409 26. Kwan, K.M. et al. *Dev. Dyn.* **236**, 3088–3099 (2007).

410

411

412